Chinese Chemical Letters 36 (2025) 110339

Contents lists available at ScienceDirect

Chinese Chemical Letters

journal homepage: www.elsevier.com/locate/cclet

Janus-type BN-embedded perylene diimides *via* a "shuffling" strategy: Regioselective functionalizable building block towards high-performance n-type organic semiconductors

Kexiang Zhao[a], Zongrui Wang[b], Qi-Yuan Wan[a], Jing-Cai Zeng[a], Li Ding[a], Jie-Yu Wang[a,*], Jian Pei[a]

[a] *Beijing National Laboratory for Molecular Sciences (BNLMS), Key Laboratory of Bioorganic Chemistry and Molecular Engineering of Ministry of Education, Center of Soft Matter Science and Engineering, College of Chemistry and Molecular Engineering, Peking University, Beijing 100871, China*
[b] *Center for Soft Matter Science and Engineering, State Key Laboratory of Organic-Inorganic Composites, Beijing University of Chemical Technology, Beijing 100029, China*

ARTICLE INFO

Article history:
Received 27 April 2024
Revised 3 August 2024
Accepted 13 August 2024
Available online 13 August 2024

Keywords:
BN heterocycles
Perylene diimides
Regioselective functionalization
Intramolecular charge transfer
N-type organic semiconductors

ABSTRACT

Regioselevtive functionalization of perylene diimides (PDIs) at bay area often requires multistep synthesis and strenuous recrystallization. Direct bromination of perylene diimides only afford the 1,6 and 1,7-regioisomers. More importantly, the 1,6-dibromo regioisomers could only be separated by preparative HPLC. Herein, we report a promising strategy for constructing Janus backbone of BN-doped perylene diimide derivatives. This Janus-type configuration results in the unique regioselective functionalization of BN-JPDIs, which yields exclusively the 1,6-regioisomers. Further investigation shows that the Janus-type configuration leads to a net dipole moment of 1.94 *D* and intramolecular charge transfer, which causes substantial changes on the optoelectronic properties. Moreover, the single crystal organic field-effect transistors based on BN-JPDIs exhibit electron mobilities up to 0.57 $cm^2\ V^{-1}\ s^{-1}$, showcasing their potential as versatile building block towards high-performance n-type organic semiconductors.

Perylene diimides (PDIs), discovered in 1913 by Kardos [1], were initially used as excellent organic pigments owing to their exceeding chemical, thermal and photochemical stability. In a long time after its discovery, derivatization of PDI scaffold was mainly focused on the imide substituents in order to tailor the solubility and solid-state packing [2,3]. It was not until the 1980s that bay functionalization of PDIs was addressed to tune their fluorescence and electronic properties [4]. Later, the *ortho* positions of PDIs were successfully functionalized taking advantage of the emerging C–H activation [5-9]. Along with the blistering development of organic electronics over the past few decades, the functionalization of PDIs as essential building blocks for organic semiconductors and fluorophores was further motivated [10-12]. Regioselective functionalization was then proposed to achieve the fine tuning of the optoelectronic properties and better device performance. However, the regioselective functionalization of perylene diimides at bay area often requires multistep synthesis and strenuous recrystallization [13,14]. Direct bromination of perylene diimides could only afford the 1,6 and 1,7-regioisomers [15]. More importantly, the 1,6-dibromo regioisomers could only be obtained by HPLC [16]. Consequently, the investigation on 1,6-regioisomers is lagging. Not only could the 1,6-regioisomers provide the platform to study the nuances of the regioisomers, they also grant us the access to new molecular and supramolecular architectures. Thus, it is of great significance to find a convenient method to regioselectively synthesize the pure 1,6-isomers.

In Roman mythology, Janus is the god of beginning and transitions depicted with two opposite faces looking to both the future and the past [17]. In the scientific community, the word "Janus" is adopted to denote the binary of two parts of different properties in one system. In sharp contrast to the well-developed Janus nanostructures, Janus-type configuration at molecular level is much less explored, especially for the Janus-type organic semiconductors which are expected to be endowed with larger molecular dipole moment, leading to stronger dipole-dipole interaction and favorable packing motif in solid state [18-21]. On the other hand, the optoelectronic properties of the Janus-type organic semiconductors remain largely unexploited. The Janus-type configuration could lower the symmetry and give rise to intramolecular charge transport (ICT) when segments with different electronegativity are

* Corresponding author.
E-mail address: jieyuwang@pku.edu.cn (J.-Y. Wang).

https://doi.org/10.1016/j.cclet.2024.110339
1001-8417/

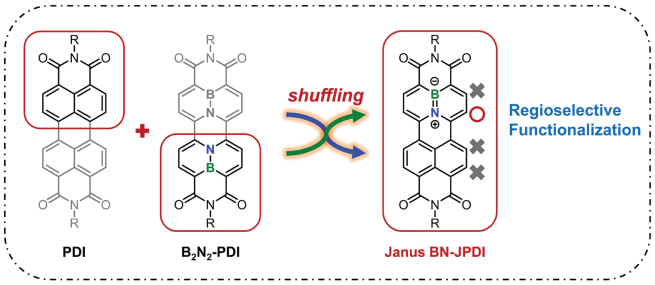

Scheme 1. Construction of Janus backbone in PDI derivatives *via* a "Shuffling" strategy.

combined in one molecule [22-24]. Most importantly, as the different parts in the Janus-type molecules might have divergent reactivities, regioselective functionalization could be achieved. The Janus configuration might be the key to the facile synthesis of 1,6-regioisomers. However, the paucity of Janus-type organic semiconductors hinders their further development [25,26].

Substitution of C=C units with isoelectronic B-N units is proved highly useful in fine tuning the optoelectronic properties of organic semiconductors [27-43]. For the majority of BN-embedded aromatics, the B-N units are inserted in a symmetrical manner, which often does not affect the overall symmetry. The asymmetrical insertion of a single B-N unit into the symmetrical scaffold, on the other hand, would result in the lowered symmetry and possibly Janus-type backbone [44-53]. Very recently, we reported the perylene diimide analogs (B_2N_2-PDIs) with two covalent B-N units located at the nodal plane, which showed interesting optoelectronic properties different from the pristine PDIs [54]. The PDI scaffold offers an excellent platform to investigate the structure-property relationship of Janus-type organic semiconductors. The asymmetrical insertion of B-N unit into the highly symmetrical PDI scaffold would result in the Janus-type backbone. The electronic effect of B-N unit in electrophilic substitution is well studied [46-50,55-57]. The bromination usually takes place at the *ortho* and *para* positions of the boron atoms. By inserting the B-N unit into the well-designed position, it is possible to take advantage of the electronic effect of B-N unit and achieve the regioselective functionalization at the bay area. Moreover, the dipolar nature of B-N unit provides local B-N dipole moment and intermolecular dipole interaction, and would give rise to even larger overall dipole moment when further combined with Janus configuration, which could lead to stronger intermolecular interaction and would be a powerful tool in constructing supramolecular architectures [58,59]. Herein, we report the synthesis and properties of another BN-embedded PDIs (BN-JPDIs) featuring Janus-type configuration and regioselective functionalization. The cross oxidative coupling of BN embedded naphthalene imide and its carbonaceous congener furnished the Janus backbone in one step from the reported molecules (Scheme 1). Compared with PDIs and B_2N_2-PDIs, the unique Janus-type configuration endues BN-JPDIs with substantial changes on their optoelectronic properties and reactivities towards electrophiles. The electron transporting ability of BN-JPDIs was evaluated by organic field-effect transistors (OFETs), exhibiting high electron mobilities up to 0.57 $cm^2 V^{-1} s^{-1}$.

The synthetic route towards BN-JPDIs is depicted in Scheme 2. Compound **1** was previously reported by our group [54] as a key intermediate for the synthesis of azaboranaphthalene monoimide (BN–NMI) with bulky substituents. It is, nevertheless, also quite useful in synthesizing BN–NMIs with less sterically hindered alkyl side chains. The yield of **2a** *via* intermediate **1** from brominated azaboranaphthalene is 69%, which is twice the yield of one-pot imidization (33%). The oxidative cross coupling between compounds **2** and **3** utilizing the *t*-BuOK/DBN pair furnished **4** in moderate yields [60-62]. Due to the competing reactions of forming the corresponding PDI analogs and B_2N_2-PDI analogs, the yields from compounds **2** to **4** are lower than the previously reported yields of B_2N_2-PDIs. It is noteworthy that the introduction of polar BN units imbues BN-embedded PDIs with higher polarity, which enables the separation of BN-JPDIs from their PDIs and B_2N_2-PDIs analogs. Consequently, **4-OE**, which has two different alkyl chains, could be conveniently acquired by this method, whereas its PDI counterpart could not due to the presence of inseparable isomers.

To achieve the regioselective functionalization, it is vital to control the position and orientation of B-N unit so that reactions could only take place at the intended bay position. By inserting the B-N unit into the long axis of the PDI scaffold, 9,10-azaboranaphthalene unit is incorporated whose reaction sites towards electrophiles are known to be the *ortho* and *para* positions of the boron atom. With the *ortho* positions being blocked by the installation of imide group, the bromination would occur at the *para* position, which is exactly the bay position of the BN-JPDI. Hence, the bromination of **4-Ph** yielded exclusively 1,6-dibromo isomer **5** with no 1,7 dibromo isomer observed on ^{1}H NMR spectrum. It is noteworthy that the bromination of PDIs with excessive bromine only gives mixtures of 1,6- and 1,7-dibromo (major) regioisomers which are inseparable by silica gel column chromatography unless specific imide substituents are chosen [15,63]. The regioselective bromination of BN-JPDIs provides a convenient access to 1,6-regioisomers which are of great significance in constructing new molecular and supramolecular architectures. To reveal the potential of **5** as a versatile building block, several Pd-catalysed cross-coupling reactions, including Suzuki, Stille, and Sonogashira coupling, were conducted and the corresponding products were isolated in good yields.

To elucidate the electronic properties of BN-JPDI, the electrostatic potential (ESP), anisotropy of the induced current density (ACID), and two-dimensional isochemical shielding surface (2D-ICSS) of BN-JPDI as well as its analogs were calculated [64-66]. The ESP map (Fig. 1a) shows positive charge located around the nitrogen atoms of BN-embedded PDIs, which is caused by the delocalization of BN units. Due to the Janus configuration of BN-JPDI, there is an obvious charge separation in the ESP map, which cannot be canceled out by symmetry and results in a net dipole moment of 1.94 *D* (Fig. 1a). In the ACID plots (Fig. 1b), clockwise ring current flows are observed over the naphthalene units indicating the aromatic feature. Upon closer inspection of the ACID plots, there is lower current density around the boron atom, which denotes the weaker shielding effect. Further analysis by 2D-ICSS (Fig. 1c) also shows the weaker aromaticity of azaboranaphthalene, especially at the boron atom. Meanwhile, the antiaromaticity of the central ring in BN-JPDI is not as strong as that in B_2N_2-PDI. The frontier molecular orbitals and energy levels of BN-JPDI were calculated (Fig. S5 in Supporting information) to further illustrate its electronic structure. Similar to B_2N_2-PDI, the internalized BN unit of BN-JPDI does not change the overall distribution of LUMO and HOMO which closely resembles that of PDI.

The electrochemical properties of BN-JPDIs were investigated by cyclic voltammetry (Table 1 and Fig. S1 in Supporting information). The LUMO energy levels of BN-JPDIs were estimated from the first half-reduction peaks to be −3.76 eV for **4-EH**, −3.75 eV for **4-Oct**, −3.73 eV for **4-pH**, and −3.75 eV for **4-OE**. It should be noted that the LUMO energy level of **4-EH** is slightly deeper relative to those of PDI-EH and B_2N_2-PDI-EH. For the HOMO energy levels, they are usually deepened by the introduction of BN units. However, **4-EH** possess similar HOMO energy level with that of PDI-EH, while B_2N_2-PDI-EH has a lowered HOMO energy level. This discrepancy is in line with the reduced optical bandgap of **4-EH** (2.26 eV), which is indicative of intramolecular charge transfer (ICT) [67].

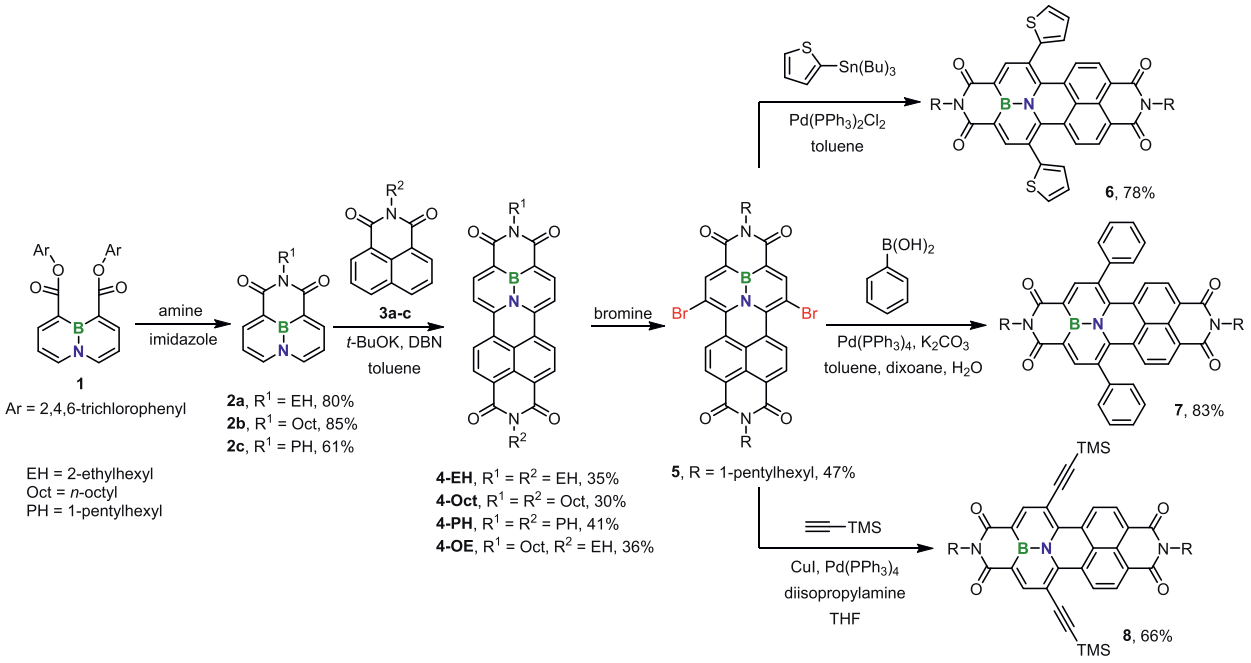

Scheme 2. The synthetic route to BN-JPDIs and their regioselective functionalization.

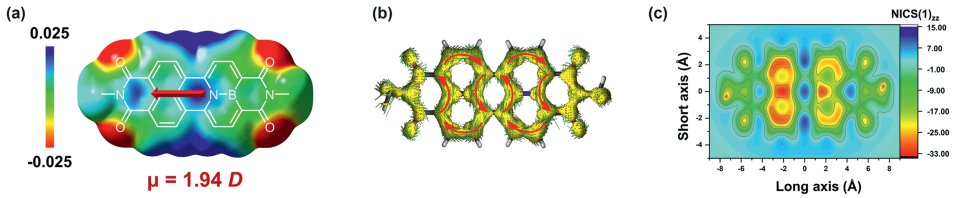

Fig. 1. (a) ESP map of BN-JPDI-Me calculated B3LYP/6–311G(d,p). The isovalue of electron density isosurface is 0.004 a.u. (b) ACID plots of BN-JPDI-Me at the isovalue of 0.035 calculated at B3LYP/6–31G(d). (c) 2D-ICSS plot of BN-JPDI-Me calculated at B3LYP/6–31+G(d). The value in the colour bar represents NICS(1)zz.

Table 1
Optoelectronic properties of BN-JPDIs.

Compound	λ_{max}^{abs} (nm)	λ_{max}^{ems} (nm)	E_g^{opt} (eV)[a]	E_{LUMO}^{CV} (eV)[b]	E_{HOMO}^{CV} (eV)[c]
4-EH	526	548	2.26	−3.76	−6.02
4-Oct	526	548	2.26	−3.75	−6.01
4-PH	526	548	2.26	−3.73	−5.99
4-OE	526	548	2.26	−3.75	−6.01
PDI-EH[d]	525	518	2.33	−3.72	−6.05
B_2N_2-PDI-EH[d]	506	534	2.41	−3.73	−6.14

[a] E_g^{opt} was calculated from 1240 nm/λ_{onset}.
[b] The first reduction potentials were measured by cyclic voltammetry (CV) in DCM using Bu_4NPF_6 as electrolyte. $E_{LUMO}^{CV} = -(E_{red}^{onset} + 4.8)$ eV.
[c] $E_{HOMO} = E_{LUMO}^{CV} - E_g^{opt}$.
[d] Taken from reference [50].

The absorption spectra of **4-EH**, PDI-EH and B_2N_2-PDI-EH are shown in Fig. 2a. The BN-JPDIs exhibit almost identical absorption characteristics as the imide substituents have little effect on their electronic structures (Fig. S2 in Supporting information). **4-EH** is chosen to compare with the corresponding PDI and B_2N_2-PDI analogues in this paragraph for simplicity's sake. Similar quartets are present at the 400–550 nm window for all three molecules on account of their analogous perylene backbones. B_2N_2-PDI-EH shows apparent hypsochromic shift (20 nm, 16 meV) in comparison with PDI-EH due to the decreased aromaticity of azaboranaphthalene units. The presence of a single B-N unit is supposed to give **4-EH** higher aromaticity and an intermediate hypsochromic shift <20 nm. However, it displayed a minor bathochromic shift (1 nm, 0.81 meV), which implies the presence of ICT. The distinguishing absorption of BN embedded perylene derivatives at 300–400 nm range is also observed for **4-EH**, which is blueshifted by 18 nm (14 meV) and has lower absorption coefficient compared to that of B_2N_2-PDI-EH [68]. The weak aromatic feature of azaboranaphthalene leads to more prominent attribute of conjugated alkene segments. This high-energy absorption band is likely to be originated from the $\pi \rightarrow \pi^*$ transition of these conjugated alkene segments [54,69]. The difference in absorption behaviors of **4-EH** and B_2N_2-PDI-EH at high-energy band could be ascribed to their different conjugated alkene segments. Excitation of **4-EH** in DCM give rise to green fluorescence (548 nm), which is more bathochromic than those of PDI-EH (534 nm) and B_2N_2-PDI-EH (518 nm). This bathochromic shift of fluorescence also substantiates the existence of ICT in BN-JPDIs. The fluorescence of **4-EH** in solvents with varying polarities were also tested (Fig. S3 in Supporting information), where **4-EH** showcased redshifted fluorescence in more polar solvents, which is in accordance with the intramolecular charge transfer. In previous reports, BN-embedded compounds with internalized BN units, such as azaborapyrene, often have lower photoluminescent quantum yields [37]. This is still valid for **4-EH** whose photoluminescence quantum yield (37%) is close to that of B_2N_2-PDI-EH (38%).

The decreased photoluminescence lifetime (Fig. 2b) of **4-EH** (2.25 ns) compared to that of B_2N_2-PDI-EH (4.98 ns) is probably caused by the ICT process in BN-JPDI [70]. To gain a deeper insight into the abosorption and ICT of BN-JPDI, we splitted the molecule into two segments as shown in Fig. 2c and calculated the charge-transport spectrum [71] to study the contributions of intrafragment electron redistributions and interfragment electron

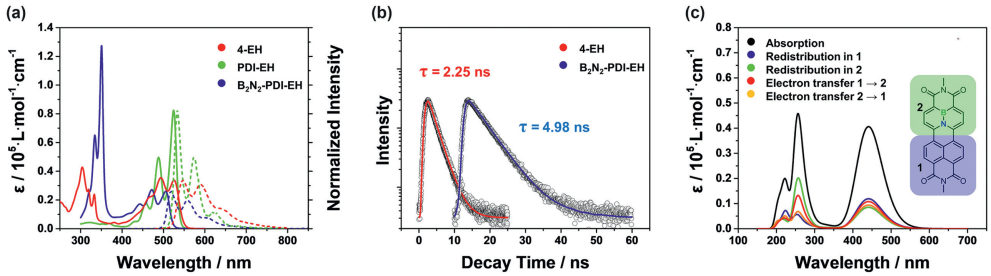

Fig. 2. (a) Absorption (solid lines) and emission spectra (dashed lines) of **4-EH** (red, excited at 460 nm), B_2N_2-PDI-EH (blue, excited at 350 nm), and PDI-EH (green, excited at 488 nm) in DCM (10^{-5} mol/L). (b) Transient photoluminescence decay of **4-EH** (red) and B_2N_2-PDI-EH (blue) in DCM (10^{-5} mol/L). (c) Calculated charge-transfer spectrum of BN-JPDI-Me at CAM-B3LYP/6–311G(d) level.

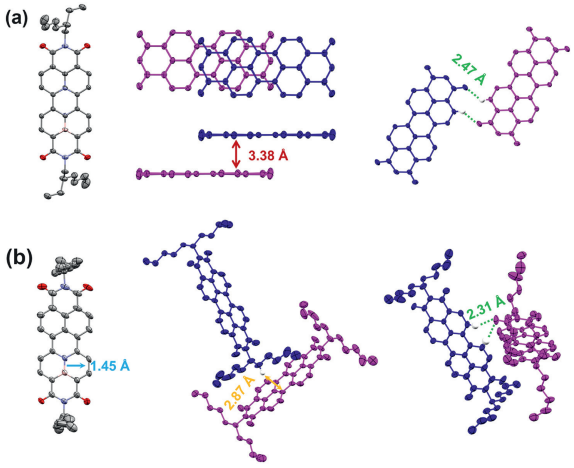

Fig. 3. Crystal structures of **4-EH** (a) and **4-PH** (b). π–π stacking distance, hydrogen bonding, B-N bond length and CH-π distance are marked in red, green, blue, and orange, respectively.

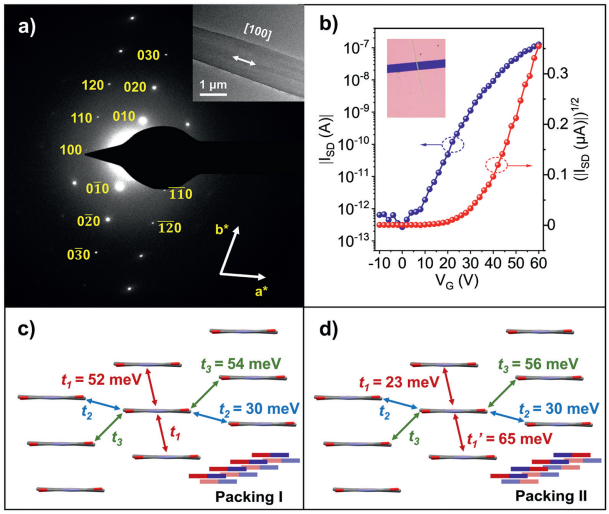

Fig. 4. (a) SAED pattern and corresponding TEM image of the single crystal micro-ribbon. (b) Transfer characteristics of the device. (c, d) Transfer integrals of two possible packing motifs of **4-EH**, calculated at PBEPBE/6–31G(d) level of theory.

transfers to the absorption spectra. The redistribution in segment **1** and electron transfer from segment **1** to segment **2** are the main contributors to the absorption at long-wavelength region, indicating the presence of ICT. However, as the contribution from redistribution and electron transfer does not differ to a great extent, the ICT of BN-JPDI is not as strong as those of well-known D-A molecules, such as 4-*N*,*N*-dimethylaminobenzonitrile (DMABN). Interestingly, the charge-transport spectrum also implies that the absorption at short-wavelength region mainly originates from the redistribution of BN-embedded segment.

To unveil the solid-state structures of BN-JPDIs, single crystals were cultivated by slow diffusion of methanol into chlorobenzene (**4-EH**) or DCM (**4-Ph**) solution. The B-N bond lengths of BN-JPDIs are around 1.45 Å, which is almost identical to that of B_2N_2-PDIs. In the crystal of **4-EH**, the BN unit and the corresponding CC unit are indistinguishable due to disorder. Slipped-cofacial columns held by strong π–π interactions are formed in the crystals of **4-EH** (Fig. 3a). These columns are further attracted by H-bonding between carbonyl oxygens and their adjacent hydrogen atoms at *ortho* positions. It is worth noting that **4-EH** has a very similar crystal structure with that of B_2N_2-PDI-EH in terms of cell parameters and molecular packing as a result of the structural resemblance. In the single crystal of **4-Ph**, π–π stacking is not observed due to the steric hindrance imposed by the 1-pentylhexyl side chains. Instead, CH-π interactions between alkyl chains and π planes are ubiquitous in the crystals with packing distances around 3.0 Å (Fig. 3b). Like **4-EH**, the carbonyl oxygens of **4-Ph** form H-bonds with the neighboring hydrogens at bay positions. Interestingly, H-bonds between carbonyl oxygens and alkyl hydrogens are also observed, which disrupts the common zig-zag arrangement of alkyl chains.

OFETs based on their micro-ribbon single crystals were fabricated to showcase the n-type charge transport properties of BN-JPDIs. As the crystal structures of **4-EH** and B_2N_2-PDI-EH are quite alike, it provides an excellent opportunity to directly compare the intrinsic charge transport properties of BN-JPDIs and B_2N_2-PDIs *via* single crystal OFETs. The micro-ribbons of **4-EH** were grown along the [100] direction, as confirmed by transmission electron microscopy (TEM) and selected area electron diffraction (SAED), which is in good accordance with the single crystal diffraction data (Fig. 4a). **4-EH** exhibits typical n-type charge carrier transport properties with a mobility up to 0.57 $cm^2\ V^{-1}\ s^{-1}$, which is higher than the electron mobility of B_2N_2-PDI-EH (0.35 $cm^2\ V^{-1}\ s^{-1}$), showing great potential of BN-JPDI as an electron-deficient building block in constructing high-performance organic optoelectronic materials. To gain more insight into the charge transport properties of **4-EH**, the exact molecular packing motif in its crystal structure is a prerequisite. There could be two kinds of packing motifs. One is parallel packing with BN units positioned at one side of the slipped-cofacial columns. The other is the antiparallel packing motif where the BN units are evenly distributed in the columns. These two packing motifs could be further divided into two subgroups where the adjacent columns adopt parallel or antiparallel packing (Fig. S7 in Supporting information). In order to understand the effect of the Janus configuration on the charge transport ability, transfer integrals between the LUMOs of **4-EH** (Figs. 4c and d) and B_2N_2-PDI-EH (Fig. S11 in Supporting information) in their packing structures were simulated using DFT calculations. It is found that the displacement of the t values of **4-EH** (30–54 meV for packing I,

23–65 meV for packing II) is much smaller than those of B_2N_2-PDI-EH (4–58 meV). Hence, the electron-transporting pathway of **4-EH** is close to multidimensional in these two packing motifs, which is favorable for effective electron transporting. Additionally, the decomposition temperatures (5% weight loss) for BN-JPDIs are as high as 440 °C for **4-OE** and 425 °C for **4-EH** (Fig. S4), which is comparable to that of PDI-EH (431 °C) and higher than that of B_2N_2-PDI-EH (389 °C). This remarkable thermal stability is crucial for their applications in organic electronics.

In summary, a series of Janus-type BN-embedded PDIs were easily synthesized from the key intermediate reported by our group in two steps. The optoelectronic properties of the obtained BN-JPDIs were investigated and compared with those of PDIs and B_2N_2-PDIs. The unique Janus-type configuration gave rise to a net dipole moment of 1.94 *D* and intramolecular charge transfer in BN-JPDIs. More importantly, BN-JPDIs allowed the regioselective functionalization to afford 1,6-regioisomers which are otherwise difficult to acquire for carbonaceous PDIs. Similar to B_2N_2-PDI, BN-JPDI also showed high unipolar n-type performance in single crystal OFETs. Our work demonstrated a facile approach to constructing Janus backbone through a "shuffling" strategy and provided a versatile building block for the high-performance n-type organic semiconductors.

Declaration of competing interest

The authors declare that they have no known competing financial interests or personal relationships that could have appeared to influence the work reported in this paper.

CRediT authorship contribution statement

Kexiang Zhao: Writing – review & editing, Writing – original draft, Methodology, Investigation, Formal analysis, Data curation. **Zongrui Wang:** Data curation. **Qi-Yuan Wan:** Data curation. **Jing-Cai Zeng:** Data curation. **Li Ding:** Data curation. **Jie-Yu Wang:** Writing – review & editing, Supervision, Resources, Project administration, Funding acquisition, Conceptualization. **Jian Pei:** Writing – review & editing, Supervision, Resources.

Acknowledgments

We are grateful to the financial support from the National Natural Science Foundation of China (Nos. 22071007, 22020102001, 22335002), the National Key R&D Program of China (No. 2022YFB3602802), and Beijing Natural Science Foundation (No. Z220025). We thank the staff, especially Dr. Zhongjie Zhu, at BL17B1 beamline of the National Facility for Protein Science in Shanghai, Shanghai Advanced Research Institute, CAS, for providing technical support in X-ray diffraction data collection. The authors acknowledge the High-Performance Computing Platform of Peking University for supporting the computational work. K. Zhao is grateful to the support of BMS Junior Fellow program. K. Zhao would also like to thank Prof. Xinxiong Li and Prof. Fei Yu for their kind assistance in X-ray diffraction data analysis.

Supplementary materials

Supplementary material associated with this article can be found, in the online version, at doi:10.1016/j.cclet.2024.110339.

References

[1] M. Kardos, Patent, DE276357C, 1913.
[2] H. Langhals, Heterocycles 40 (1995) 477–500.
[3] S. Demmig, H. Langhals, Chem. Ber. 121 (1988) 225–230.
[4] G. Seybold, G. Wagenblast, Dye. Pigm. 11 (1989) 303–317.
[5] S. Nakazono, Y. Imazaki, H. Yoo, et al., Chem. Eur. J. 15 (2009) 7530–7533.
[6] J.E. Bullock, M.T. Vagnini, C. Ramanan, et al., J. Phys. Chem. B 114 (2010) 1794–1802.
[7] G. Battagliarin, C. Li, V. Enkelmann, K. Müllen, Org. Lett. 13 (2011) 3012–3015.
[8] T. Teraoka, S. Hiroto, H. Shinokubo, Org. Lett. 13 (2011) 2532–2535.
[9] J. Wu, D. He, L. Zhang, et al., Org. Lett. 19 (2017) 5438–5441.
[10] W. Jiang, Z. Wang, J. Am. Chem. Soc. 144 (2022) 14976–14991.
[11] N. Liang, D. Meng, Z. Wang, Acc. Chem. Res. 54 (2021) 961–975.
[12] A. Nowak-Krol, F. Wurthner, Org. Chem. Front. 6 (2019) 1272–1318.
[13] G. Shao, M. Wu, X. Wang, et al., J. Org. Chem. 87 (2022) 14825–14832.
[14] S. Sengupta, R.K. Dubey, R.W.M. Hoek, et al., J. Org. Chem. 79 (2014) 6655–6662.
[15] F. Würthner, V. Stepanenko, Z. Chen, et al., J. Org. Chem. 69 (2004) 7933–7939.
[16] M. Ball, Y. Zhong, B. Fowler, et al., J. Am. Chem. Soc. 138 (2016) 12861–12867.
[17] M. Gagarin, The Oxford Encyclopedia of Ancient Greece and Rome, Oxford University Press, 2010.
[18] K. Miyazaki, K. Matsuo, H. Hayashi, et al., Org. Lett. 25 (2023) 7354–7358.
[19] X. Song, L. Hou, R. Guo, ACS Appl. Mater. Interfaces 13 (2021) 2961–2970.
[20] A. Marsh, E.G. Nolen, K.M. Gardinier, J.M. Lehn, Tetrahedron Lett. 35 (1994) 397–400.
[21] M. Mas-Torrent, C. Rovira, Chem. Rev. 111 (2011) 4833–4856.
[22] R. Misra, S.P. Bhattacharyya, Intramolecular Charge Transfer: Theory and Applications, Wiley, 2018.
[23] Y. Li, T. Liu, H. Liu, M.Z. Tian, Y. Li, Acc. Chem. Res. 47 (2014) 1186–1198.
[24] E. Aqad, M.V. Lakshmikantham, M.P. Cava, R.M. Metzger, V. Khodorkhovsky, J. Org. Chem. 70 (2005) 768–775.
[25] Y. Zhang, Y. Wang, C. Gao, et al., Chem. Soc. Rev. 52 (2023) 1331–1381.
[26] C. Wang, H. Dong, W. Hu, Y. Liu, D. Zhu, Chem. Rev. 112 (2012) 2208–2267.
[27] J. Wang, A. Zheng, Y. Xiang, J. Liu, J. Am. Chem. Soc. 145 (2023) 14912–14921.
[28] X. Chen, D. Tan, D.T. Yang, J. Mater. Chem. C 10 (2022) 13499–13532.
[29] J. Lee, H. Kim, H. Park, et al., J. Am. Chem. Soc. 143 (2021) 11180–11190.
[30] T. Sakamaki, T. Nakamuro, K. Yamashita, et al., Chem. Mater. 33 (2021) 5337–5344.
[31] F.D. Zhuang, Z.H. Sun, Z.F. Yao, et al., Angew. Chem. Int. Ed. 58 (2019) 10708–10712.
[32] S. Nakatsuka, N. Yasuda, T. Hatakeyama, J. Am. Chem. Soc. 140 (2018) 13562–13565.
[33] J. Dosso, J. Tasseroul, F. Fasano, et al., Angew. Chem. Int. Ed. 56 (2017) 4483–4487.
[34] J.Y. Wang, J. Pei, Chin. Chem. Lett. 27 (2016) 1139–1146.
[35] X.Y. Wang, A. Narita, X. Feng, K. Müllen, J. Am. Chem. Soc. 137 (2015) 7668–7671.
[36] X.Y. Wang, H.R. Lin, T. Lei, et al., Angew. Chem. Int. Ed. 52 (2013) 3117–3120.
[37] M.J.D. Bosdet, W.E. Piers, T.S. Sorensen, M. Parvez, Angew. Chem. Int. Ed. 46 (2007) 4940–4943.
[38] T. Kaehler, M. Bolte, H.W. Lerner, M. Wagner, Angew. Chem. Int. Ed. 58 (2019) 11379–11384.
[39] O. Ouadoudi, T. Kaehler, M. Bolte, H.W. Lerner, M. Wagner, Chem. Sci. 12 (2021) 5898–5909.
[40] Ö. Seven, S. Popp, M. Bolte, H.W. Lerner, M. Wagner, Dalton Trans. 43 (2014) 8241–8253.
[41] Y. Wang, K. Zhang, F. Chen, et al., Chin. J. Chem. 40 (2022) 2671–2677.
[42] L. Li, Y. Gao, C. Dou, J. Liu, Chin. Chem. Lett. 31 (2020) 1193–1196.
[43] X. Long, C. Dou, J. Liu, L. Wang, Chin. Chem. Lett. 29 (2018) 1343–1346.
[44] E. Sans-Panadés, J.J. Vaquero, M.A. Fernández-Rodríguez, P. García-García, Org. Lett. 24 (2022) 5860–5865.
[45] Y. Zhang, W. Li, R. Jiang, et al., J. Org. Chem. 87 (2022) 12986–12996.
[46] A. Abengózar, I. Valencia, G.G. Otárola, et al., Chem. Commun. 56 (2020) 3669–3672.
[47] C. Zhang, L. Zhang, C. Sun, W. Sun, X. Liu, Org. Lett. 21 (2019) 3476–3480.
[48] A. Abengózar, D. Sucunza, P. García-García, et al., J. Org. Chem. 84 (2019) 7113–7122.
[49] A. Abengózar, P. García-García, D. Sucunza, et al., Org. Lett. 21 (2019) 2550–2554.
[50] A. Abengózar, P. García-García, D. Sucunza, et al., Org. Lett. 19 (2017) 3458–3461.
[51] J.S.A. Ishibashi, A. Dargelos, C. Darrigan, A. Chrostowska, S.Y. Liu, Organometallics 36 (2017) 2494–2497.
[52] M.J.S. Dewar, W.H. Poesche, J. Org. Chem. 29 (1964) 1757–1762.
[53] M.J.S. Dewar, V.P. Kubba, R. Pettit, J. Chem. Soc. (1958) 3073–3076.
[54] K. Zhao, Z.F. Yao, Z.Y. Wang, et al., J. Am. Chem. Soc. 144 (2022) 3091–3098.
[55] F. Sun, L. Lv, M. Huang, Z. Zhou, X. Fang, Org. Lett. 16 (2014) 5024–5027.
[56] I. Valencia, P. García-García, D. Sucunza, F. Mendicuti, J.J. Vaquero, J. Org. Chem. 86 (2021) 16259–16267.
[57] L. Zi, J. Zhang, C. Li, et al., Org. Lett. 22 (2020) 1499–1503.
[58] L. Brunsveld, B.J.B. Folmer, E.W. Meijer, R.P. Sijbesma, Chem. Rev. 101 (2001) 4071–4098.
[59] S. Chen, P. Slattum, C. Wang, L. Zang, Chem. Rev. 115 (2015) 11967–11998.
[60] T. Sakamoto, C. Pac, J. Org. Chem. 66 (2001) 94–98.
[61] H. Langhals, S. Christian, A. Hofer, J. Org. Chem. 78 (2013) 9883–9891.
[62] L. Chen, C. Li, K. Müllen, J. Mater. Chem. C 2 (2014) 1938–1956.
[63] J. Ma, L. Yin, G. Zou, Q. Zhang, Eur. J. Org. Chem. 2015 (2015) 3296–3302.
[64] D. Geuenich, K. Hess, F. Köhler, R. Herges, Chem. Rev. 105 (2005) 3758–3772.
[65] T. Lu, F. Chen, J. Comput. Chem. 33 (2012) 580–592.

[66] S. Klod, E. Kleinpeter, J. Chem. Soc., Perkin Trans. 2 (2001) 1893–1898.
[67] A. Slama-Schwok, M. Blanchard-Desce, J.M. Lehn, J. Phys. Chem. 94 (1990) 3894–3902.
[68] P.F. Zhang, J.C. Zeng, F.D. Zhuang, et al., Angew. Chem. Int. Ed. 60 (2021) 23313–23319.
[69] X. Fang, Molecules 26 (2021) 7148–7157.
[70] C.C. Wu, E.Y. Li, P.T. Chou, Chem. Sci. 13 (2022) 7181–7189.
[71] Z. Liu, X. Wang, T. Lu, A. Yuan, X. Yan, Carbon 187 (2022) 78–85.